Low-temperature phase separation of a binary liquid mixture in porous materials studied by cryoporometry and pulsed-field-gradient NMR

Rustem Valiullin* and István Furó†
Division of Physical Chemistry, Department of Chemistry, Royal Institute of Technology, SE-10044 Stockholm, Sweden
(Received 15 May 2002; published 25 September 2002)

The low-temperature liquid-liquid phase separation of the partially miscible hexane-nitrobenzene mixture imbibed in porous glasses of different pore sizes from 7 to 130 nm has been studied using ^{1}H NMR (nuclear magnetic resonance) cryoporometry and pulse field gradient NMR methods. The mixture was quenched below both its upper critical solution temperature (T_{cr}) and the freezing point of nitrobenzene. The size distribution of frozen nitrobenzene domains was derived through their melting point suppression according to the Gibbs-Thompson relation. The obtained data reveal small initial droplets of nitrobenzene surrounded by hexane, which are created as the temperature is decreased below T_{cr} and which thereafter coalesce by a droplet-diffusion mechanism. The inter-relation between the pore size and the found size distribution and shapes of nitrobenzene domains is discussed, as well as several aspects of molecular self-diffusion.

DOI: 10.1103/PhysRevE.66.031508 PACS number(s): 64.70.Ja, 61.43.Gt, 82.56.−b

I. INTRODUCTION

The behavior of critical binary liquids confined in porous materials has attracted theoretical and experimental attention over a long period [1–26]. Differences in the liquid-solid surface interaction between the mixture components and the effect of confinement lead to new phenomena as compared to bulk mixtures. For example, shifts of the critical parameters in confined space, such as the critical temperature and the critical composition, take place for most of the investigated systems [1–6,8]. Together with modification of the static properties, one also observed slowing down of phase-separation kinetics, leading to a metastable liquid-liquid (LL) microphase equilibrium on the laboratory time scale [8–12,14].

Theoretically, these observations are usually described either by the random field Ising (RFIM) [15,16] or by the single-pore (SPM) [17] models. The heterogeneity of the solid matrix is described in RFIM as a short-ranged random field acting on the liquid mixture, whereas the SPM is constructed by considering the wetting behavior of the mixture components in a single cylindrical pore. With respect to the porous materials with a random structure, such as controlled porous glasses (CPG from CPG, Inc., Vycor from Corning), it is not straightforward to prefer one model above other: If the features of the SPM can only be realized on the short length scales of order of the pore size, the large-scale properties can be taken into account only in the frame of RFIM. At the same time, both approaches predict the existence of wetting layers of one preferentially adsorbed component under certain conditions, and slow phase-separation kinetics, leading to inaccessibility of the macroscopic phase separation on a measurable time scale. These features were also confirmed in computer simulation studies of liquid mixtures in simple geometries [9–12,18]. It was found that in the two-phase region, intrapore liquid forms a set of microscopic domains of size and form similar to that of the confining pores; depending on the geometry of a solid matrix and details of liquid-solid interaction, either plug or capsule configuration (a plug fills a pore completely, while the capsule occupies the interior of the pore separated by liquid from the pore walls, see Ref. [9] for exact definition) can be obtained. Note that, as yet, there is no significant experimental evidence for such a behavior. These domains tend to grow very slowly with time. Most experimental studies also confirm complete wetting of a solid wall by one of the liquids. The inner phase is found to have a characteristic size of order [6,22] or exceeding the pore size [19,20].

If all the above prescribed results state at least the existence of the microscopic domains with different compositions and distinct interfaces, high-resolution nuclear magnetic resonance (NMR) spectra together with some self-diffusion data in the aniline-cyclohexane mixture in Vycor porous glass were interpreted in terms of no discernible microscopic phase separation [23]. Instead, ''the presence of continuous spatial variations of composition without distinct interfaces'' was concluded, which is inconsistent with both the RFIM and the SPM. Alternatively, the slow kinetics of phase separation was explained by taking into account only the relatively low mutual diffusion coefficient for immiscible liquids [24].

To date, neither theoretical nor experimental studies suggest macroscopic (that is, continuous liquid domains much exceeding the pore size) phase separation inside random porous structures. Except this particular point, no agreement has been reached as concerning other details of LL equilibrium in porous matrix. Manifestation of the phase separation in small pores less than 10 nm, the microgeometry of the forming domains and their size distribution all fall into this category. From the experimental point of view, difficulties in studying such aspects are caused by the complex properties of the porous materials. Well-established techniques for investigating phase separation, such as light scattering, are lim-

*Permanent address: Department of Molecular Physics, Kazan State University, Russia.
†Author to whom correspondence should be addressed; email address: ifuro@physchem.kth.se

ited due to either the opacity or diffuse scattering and the evaluation of experimental data obtained using scattering methods is also complicated by the background scattering from the random solid matrix.

Recently, an experimental method utilizing NMR spectroscopy has been proposed to probe the structure of the phase-separated liquids in a porous matrix [26]. The whole procedure consists of the following steps.

(1) Cooling a binary mixture of partially miscible liquids *A* and *B* to a temperature T^* that is far below both the upper critical solution temperature T_{cr} and the freezing point of one of its component T_{fr}^B. Here, it is assumed that the mixture components were chosen in such a way that they are characterized by the different freezing temperatures, and the condition $T_{fr}^A < T_{fr}^B < T_{cr}$ is fulfilled. Under this condition one first obtains a LL separation upon lowering the temperature. On further cooling below T_{fr}^B, domains of the *B*-rich phase freeze but, for $T^* > T_{fr}^A$, *A*-rich domains remain liquid.

(2) After the mixture reaches the state with frozen *B* component, it is then slowly warmed, leading to melting of the frozen *B*-rich domains (referred below also as crystals). For a crystal of diameter d this occurs at the temperature $T_m(d)$ suppressed with respect to that in bulk mixture T_m as given by the Gibbs-Thompson relation [27]

$$T_m - T_m(d) = \frac{4\sigma T_m}{\triangle H_f \rho d} \equiv \frac{K}{d}, \tag{1}$$

where σ is the surface energy of solid-liquid interface, $\triangle H_f$ is the bulk enthalpy of fusion, and ρ is the crystal density. Since NMR signals from liquid and crystal can be easily distinguished due to the very large difference in their respective transverse relaxation rates R_2, the crystal-size distribution function can be derived from the variation of the liquid NMR signal according to Eq. (1). The NMR version of conventional thermoporometry methods [28], known also in the literature as NMR cryoporometry [29,30], gives some advantages with respect to the objects under study. It allows not only to investigate the characteristics of the melting process, but also to directly quantify the fraction of the molecules in the liquid phase and perform various NMR experiments on different molecules by exploiting differences in chemical shifts.

In Ref. [26], the prescribed method has been applied to study phase separation of a binary liquid mixture of nitrobenzene and *n*-hexane of critical composition in porous glasses of 24 and 73 nm. Anticipating that freezing of the nitrobenzene-rich domains at low temperatures do not change the relative geometrical structure of the phase-separated liquids, the nitrobenzene domain-size distribution functions in both porous glasses have been obtained. Shape features were explained by considering a droplet coalescence mechanism below the critical temperature. In order to clarify the validity of conclusions in Ref. [26], in the present study we investigate phase separation in porous glasses of broader size range, from 7.5 to 127.3 nm. Pulsed field gradient NMR has been proved to be a useful noninvasive method to study details of molecular dynamics in porous materials [31,32] and also can give useful information on porous space modified by embedded frozen domains [33]. Thus, results of a more detailed pulsed field gradient NMR study of critical as well as off-critical mixtures in porous glasses will also be provided below.

TABLE I. Physical properties of the controlled porous glasses used in the present study supported by the manufacturer (CPG, Inc.).

Label	d_0 [a]	Δd [b]	S [c]	V [d]
*G*7	7.5	6.0	140.4	0.47
*G*24	23.7	4.3	78.8	0.95
*G*73	72.9	6.4	24.9	0.75
*G*127	127.3	8.4	24.3	1.19

[a]Mean pore diameter (nm).
[b]80% of pores are within the given range with respect to d_0.
[c]Specific surface (m^2/g).
[d]Specific pore volume (10^{-6} m^3/g).

II. MATERIALS AND METHODS

Binary mixtures of nitrobenzene ($C_6H_5NO_2$, Lancaster Synthesis, 99%) and *n*-hexane (C_6H_{14}, Merck, 99%) with near-critical volume fraction of nitrobenzene $\phi_{NB} = 0.36 \pm 0.02$ have been used. The critical mixture is known to have the upper critical solution temperature $T_{cr} = 293.1$ K [34]. The freezing temperatures for the pure nitrobenzene and hexane are $T_{fr}^{NB} = 278.9$ K and $T_{fr}^{HX} = 178.2$ K, respectively. Uncoated controlled porous glasses (CPG), prepared by a spinodal decomposition process, of mean pore size from 7.5 to 127.3 nm (Table I) were obtained from CPG, Inc. (Lincoln Park). All CPGs were specified by the manufacturer to consist of near-spherical particles of 120–150 μm that have highly networked intraparticle porous structure with a narrow distribution of pore diameters. Data from the manufacturer on some properties of the glasses used, such as mean pore diameter d_0, pore-size distribution, surface area *S*, and specific volume *V*, are given in Table I. The liquid mixtures have been imbibed into CPG at relatively high temperature $T = 323$ K $> T_{cr}$, to avoid introduction of a concentration inhomogeneity during imbibition. The filling factor was chosen to provide a complete saturation of only the intraparticle porous space. Before measurements the samples were equilibrated at $T = 340$ K in the one-phase region for 24 h. Some additional experiments were also performed with off-critical concentration mixtures ($\phi_{NB} = 0.2 \pm 0.02$ and $\phi_{NB} = 0.6 \pm 0.02$) prepared in the same way.

The ^{1}H NMR measurements were carried out on a Bruker DMX-200 spectrometer equipped with a BVT-3000 temperature controller with a reproducibility and stability better than ± 0.1 K. Before the measurements the temperature points were calibrated using two independent *in situ* Pt(100) platinum resistors. The ^{1}H NMR cryoporometry experiments were performed using the $90° - \tau - 180°$ spin-echo pulse sequence with $\tau = 5$ ms, which was sufficient to exclude the NMR signal from the crystal phase due to short spin-spin relaxation times there. The time-domain signal collected af-

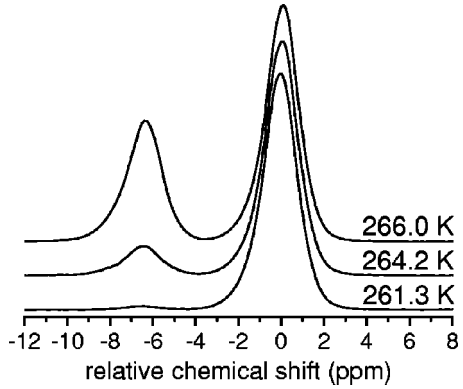

FIG. 1. The ^{1}NMR spectra of the nitrobenzene-hexane critical mixture as a function of increasing temperature in porous glass of 24-nm ($G24$) pore diameter. The nominal chemical shift scale is set by rendering the hexane peak (right) to 0 ppm, which provides the nitrobenzene peak (left) at $\sim$6.5 ppm.

ter the echo top was Fourier transformed to provide spectra as shown in Fig. 1. As can be seen, NMR signals from the nitrobenzene and hexane molecules can be distinguished due to the difference in their ^{1}H proton chemical shifts ($\approx$6.5 ppm). Starting at the temperatures above T_{cr} samples were cooled at a rate of 0.2 K/min until the nitrobenzene phase froze (this was controlled by the absence of nitrobenzene line in spectra recorded by the spin-echo pulse sequence). The intensity I of the nitrobenzene line was then recorded as a function of slowly increasing temperature T (heating between two subsequent temperature points at which measurements were performed was at a rate of 0.1 K/min) with 5-min equilibration time that corresponds to NMR measurement at the particular temperature.

The function $I(T)$ reflects the number of nitrobenzene molecules in liquid state (the signal from the crystalline phase is removed by choosing sufficiently long spin-echo time τ). Recalling that the melting temperature depends on crystal dimension through Eq. (1), the crystal-size distribution function $P(d)$, that provides the volume of crystals with minimum dimension d, is readily obtained as

$$P(d)=\frac{\partial I}{\partial T}\frac{K}{d^2}. \tag{2}$$

Details of derivation of Eq. (2) are given in Ref. [29]. First, the derivative of the liquid NMR intensity $I(T)$ by temperature provides nitrobenzene crystal volume as function of the melting temperature for a particular crystal size. The factor K/d^2 rescales the abscissa to provide a true size distribution. $P(d)$ obtained in this way is a normalizable size distribution function; its integral gives the total volume occupied by nitrobenzene molecules as is demonstrated in Fig. 2, where the NMR intensity I at high temperatures is proportional to the total nitrobenzene volume.

It is worthwhile noting that in the derivation of Eq. (1) the approximation $\ln[T_m(d)/T_m]\approx[T_m-T_m(d)]/T_m$ has been used (see, for example, Ref. [35]). If this approximation is not made for small crystals with a large shift in the melting temperature from the bulk value, one obtains the more general relation

$$P(d)=\frac{\partial I}{\partial T}\frac{K}{d^2}\exp\left(-\frac{K}{dT_m}\right). \tag{3}$$

Fourier transform pulsed field gradient NMR measurements [36] using a probe producing pulsed field gradients up to 9.6 T/m were performed in the same manner as NMR cryoporometry experiments with respect to the temperature. In order to reduce the influence of magnetic field inhomogeneity in the samples with porous glasses, a ''13-interval'' stimulated echo pulse sequence with the two gradient pulses of opposite signs was used [37]. The typical values for the gradient pulse duration δ and distance τ_1 between the first and second 90° radiofrequency pulses were 1.0 and 5.0 ms, respectively. The original registered quantity in pulsed field gradient spin-echo NMR experiments is the incoherent scattering function $S(q,t_d)$, where $q=\gamma\delta g$ is defined by the magnitude of the magnetic field gradient pulses g, the nucleus gyromagnetic ratio γ, and the effective diffusion time t_d. During the experiments, q was scaled by changing the magnitude of g and keeping δ constant. The diffusion damping of the normalized stimulated-echo amplitude $S(q,t_d)$ in a pure liquid with the self-diffusion coefficient D_0 is expressed as

$$S(q,t_d)\equiv\frac{A(q,t_d)}{A(0,t_d)}=\exp(-q^2D_0t_d), \tag{4}$$

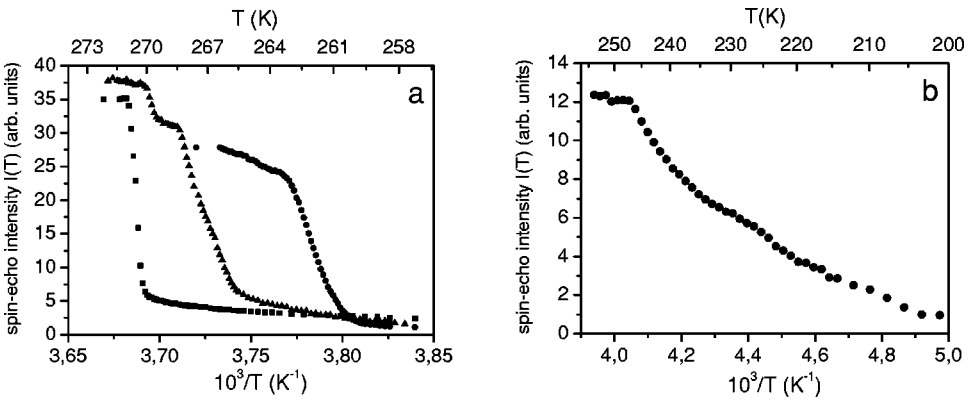

FIG. 2. NMR spin-echo intensity I of the nitrobenzene component in the mixture with critical composition as a function of increasing temperature in porous glasses of (a) 24-nm ($G24$, circles), 73-nm ($G73$, triangles), and 127-nm ($G127$, squares) and (b) 7.5-nm (G7) pore diameter.

where $A(q,t_d)$ and $A(0,t_d)$ is the stimulated-echo signal intensities with and without applied magnetic field gradient, respectively. If the system consists of nuclei having different diffusion constants, then $S(q,t_d)$ is the sum of terms given by Eq. (4) with the appropriate weighting factors. Often, experimentally registered functions $S(q,t_d)$ do not follow a single-exponential law, due to complex relaxation mechanisms or non-Gaussian dynamics [38,39]. In this case, one may describe the system by the average diffusion coefficient D, which is experimentally obtained from the slope to $S(q,t_d)$ at small magnitudes of q:

$$D=-\frac{1}{t_d}\left(\frac{\partial S(q,t_d)}{\partial q^2}\right)_{q\to 0}. \tag{5}$$

In what follows, the term ''diffusion coefficient'' will refer to this average value, unless otherwise stated.

III. EXPERIMENTAL RESULTS

Recapitulation of previous findings. In the subsequent discussion, we rely on some results that were firmly established in our previous paper [26].

(1) There remains a small (in the order of a percent) amount of hexane in the nitrobenzene phase and vice versa below the phase separation. As one consequence, the bulk melting temperature of the nitrobenzene-rich phase shifts ($T^{NB}_{m,mix}=272.5\pm 0.2$ K) from that in pure nitrobenzene ($T^{NB}_{fr}=278.9$ K).

(2) Because of supercooling, the nitrobenzene-rich phase freezes far below this temperature. The samples (with the exception of smallest pore size, see below) were kept at ~ 250 K in order to freeze the nitrobenzene-rich phase.

(3) For a bulk liquid mixture, the phase separation below T_{cr} results in two discernible liquid columns, located over each other in the NMR tube.

A. NMR cryoporometry

Critical mixture in 24-, 73-, and 127-nm pores. Definitive freezing of the nitrobenzene part was observed in the samples with the porous glasses $G24$, $G73$, and $G127$ in the temperature range $246-252$ K (no correlation between the pore size and freezing temperature was observed). This was demonstrated by a sudden and large decrease of the nitrobenzene NMR line intensity in the spectra (to about 2–3 % of its initial signal intensity) recorded by the $90°-\tau-180°$ pulse sequence with $\tau=5$ ms. In Fig. 1, we show some NMR spectra obtained for the sample $G24$ at different temperatures *during warming*. It is also seen from the figure that the hexane signal intensity is roughly temperature independent. The melting of the nitrobenzene domains in pores is spread over broad temperature range depending on the pore size, which is demonstrated in Fig. 2(a) by the NMR spin-echo signal intensities of the nitrobenzene component as a function of temperature.

Critical mixture in 7.5-nm pores. In contrast to the porous glasses of larger pore sizes in the CPG sample of 7.5-nm pore diameter, the nitrobenzene line intensity monotonically decreases with lowering the temperature starting from ~ 240 K down to the lowest investigated temperature $T=200$ K. Importantly, we checked upon warming as the temperature was kept constant, the signal remained unchanged with time (up to 2 h). The nitrobenzene signal intensity measured upon warming is shown in Fig. 2(b).

Domain-size distributions. The size distribution of the frozen domains that causes spreading of the melting temperatures can be obtained from the data in Fig. 2 through Eqs. (2) or (3). In these equations the unknown parameter K for our particular mixture may be estimated as follows. The bulk enthalpy of fusion $\triangle H_f$ for pure hexane and nitrobenzene (13.1 kJ/mol [40] and 12.1 kJ/mol [41], accordingly) are close and one can plausibly assume that the nitrobenzene $\triangle H_f$ in the mixture will remain unchanged. Because of near immiscibility of the hexane and nitrobenzene at these temperatures (far below T_{cr}), the surface energy σ of the progressing liquid-solid interface is controlled mostly by the nitrobenzene molecules. As concerning the initiation of melting, the presence of liquidlike layers of nitrobenzene on the nitrobenzene-rich crystals is indicated in a number of molecular dynamics studies of crystallization process (see, for example, Refs. [42,43]). Hence, we can estimate K to have approximately the same value $K\approx 125$ K nm [44] as for the pure nitrobenzene (the validity of this approximation will also be discussed below).

Taking into account the suppressed value of the bulk melting point, $T_m=T^{NB}_{m,mix}=272.5\pm 0.2$ K, the obtained domain-size distribution functions $P(d)$ are shown in Fig. 3 as evaluated using Eq. (2). For the sample with the smallest pore diameter 7.5 nm, the domain-size distribution obtained using Eq. (3) is also shown with no significant difference from the former. For comparison, the NMR cryoporometry results [raw intensity data not shown, evaluated with $K=125$ K nm [44] and $T^{NB}_{fr}=278.9$ K via Eq. (2)] from pure nitrobenzene imbibed in CPGs and providing the pore-size distribution functions are shown in Fig. 3 by the dashed lines. Note that the observed peaks of these distribution functions are within 10% of the nominal pore sizes provided by the manufacturer.

Two additional experiments, aimed at controlling the effect of the experimental procedure itself on the obtained size distributions were also performed. In the first experiment, the samples were kept for several hours at temperatures below T_{cr} but above T^{NB}_{fr}. Thereafter, the procedure continued with freezing of the nitrobenzene-rich domains as described above. In the second experiment, after the melting step, we have repeated the freezing/melting of the sample starting from $T=275.0$ K (below T_{cr}) and obtained data on the repeated melting. Importantly, the results from these experiments were identical within experimental error to those obtained as described in the previous paragraphs.

B. Pulsed field gradient NMR

$S(q,t_d)$ for the nitrobenzene and hexane in the *bulk* mixture at temperatures below T_{cr}, but the nitrobenzene-rich phase still unfrozen, have been found to slightly deviate from

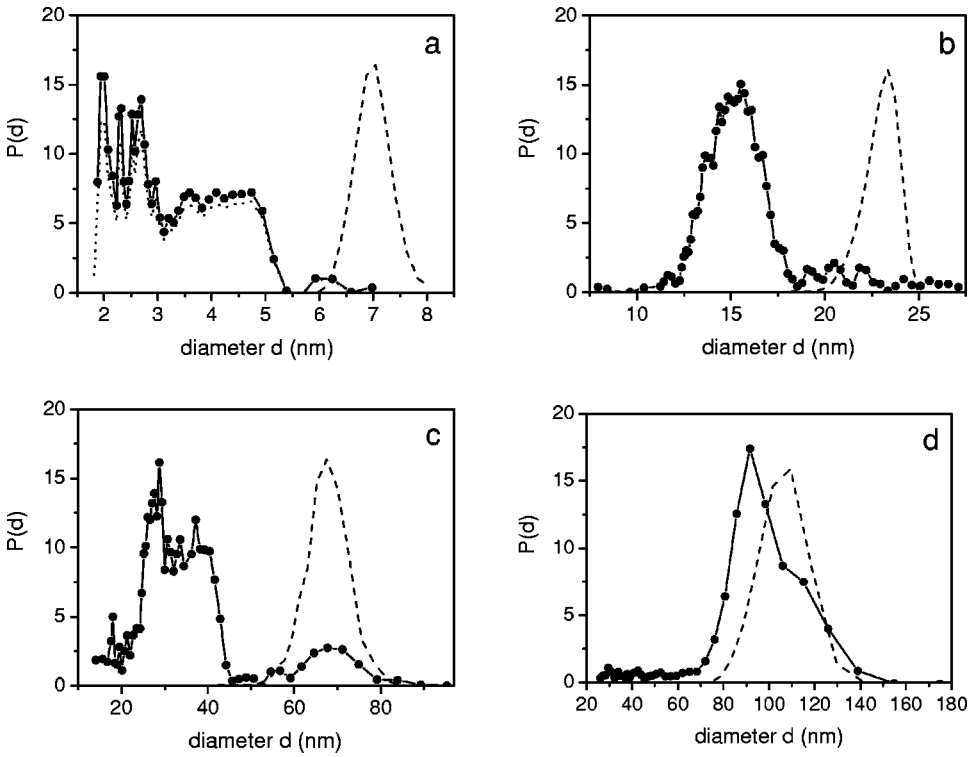

FIG. 3. Nitrobenzene domain-size distribution functions $P(d)$ in the mixture with critical composition in porous glasses of (a) 7.5-nm, (b) 24-nm, (c) 73-nm ($G73$), and (d) 127-nm pore diameters obtained from the NMR cryoporometry data in Fig. 2. The dashed lines represent the pore-size distribution functions obtained using pure nitrobenzene as a probe liquid. The dotted line in (a) is the domain-size distribution function evaluated using Eq. (3) (see the text for details). Vertical axis is in arbitrary units.

the exponential form given by Eq. (4), as shown in Fig. 4 for the hexane component. This observation reflects the difference in mobilities of the molecules in the upper hexane-rich and lower nitrobenzene-rich phases [45] that are, *in bulk*, in slow molecular exchange on the NMR time scale. In contrast, for mixtures imbibed in CPGs, $S(q,t_d)$ are characterized by single exponential decays (Fig. 4) which do not depend on t_d in the interval from 10 to 640 ms. The same behavior has also been observed for the hexane component of the mixture in porous glasses when the nitrobenzene part was frozen: $S(q,t_d)$ were monoexponential and coincided in the range of diffusion times t_d from 10 to 160 ms.

The values of the average self-diffusion coefficients D of the mixture components at different temperatures during warming and obtained using Eq. (5) are shown in Fig. 5. The

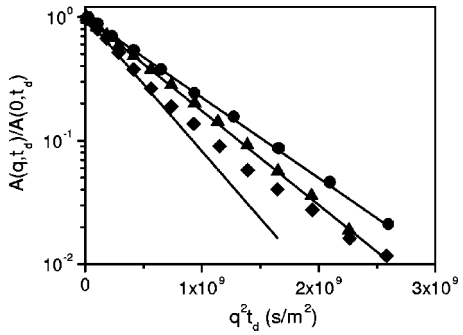

FIG. 4. Normalized NMR scattering functions for the hexane component in the mixture with critical composition measured at $t_d=10$ ms in bulk (diamonds) and in porous glasses of 24-nm ($G24$, circles) and 73-nm ($G73$, triangles) at $T=280$ K. Solid lines represent the slopes to small-q region of $A(q,t_d)$ according to the Eq. (5).

dashed lines represent the Arrhenius law

$$D(T)=A\exp(-E_D/RT), \tag{6}$$

with the parameters given in the figure caption. At low temperatures the diffusivity of the hexane and nitrobenzene molecules in the *bulk* mixture are comparable [45] and behave similarly with the increase of temperature. As the melting point of nitrobenzene is reached, the diffusion coefficient for the nitrobenzene molecules abruptly falls by about a factor of 3. This observation reflects the fact that after melting we register mostly the NMR signal from the nitrobenzene-rich molten phase with lower mobility [45].

Some differences, both to the bulk and among the two molecular species, are observed in the mixtures in CPGs. The self-diffusion coefficient D_{HX} of the hexane molecules in CPGs are lower than in the bulk mixture (see, for example, Fig. 5) due to confinement caused by the solid glass matrix and the intermitting nitrobenzene domains. The temperature dependences $D_{HX}(T)$ are relatively monotonic in the whole investigated temperature and concentration ranges, and also shown in Fig. 6 for the porous glass of 24-nm pore diameter (for the other porous glasses the results were qualitatively the same). In contrast, $D_{NB}(T)$ in CPGs decreased on melting, which is again a consequence of nitrobenzene molecules having a lower diffusion coefficient in liquid nitrobenzene than in liquid hexane [26]. This also explains the close values of $D_{NB}(T)$ in different samples at high temperatures: while hexane molecules are confined both by the walls and by the nitrobenzene domains, the diffusion of nitrobenzene molecules *increases* upon entering into the hexane domains.

In order to check our supposition that the structure of the nitrobenzene domains is preserved during freezing, we have

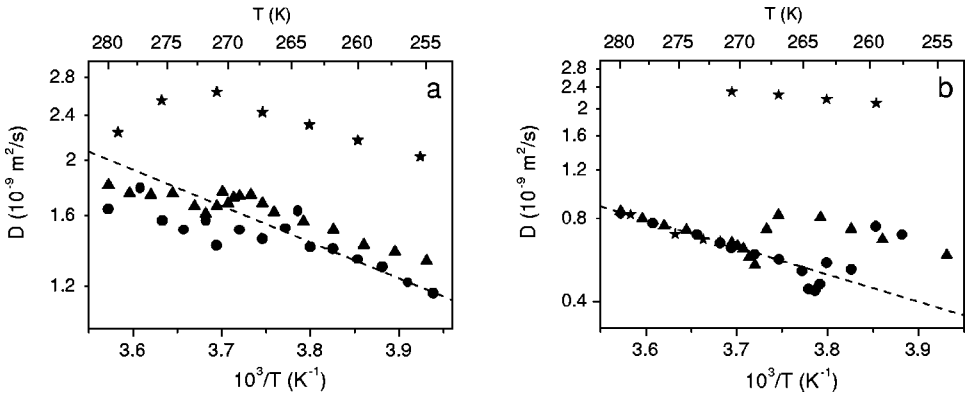

FIG. 5. Average self-diffusion coefficients for the hexane (a) and nitrobenzene (b) in the mixture with critical composition in bulk (stars) and in porous glasses of 24-nm ($G24$, circles) and 73-nm ($G73$, triangles) pore diameters. The dashed lines are Eq. (6) with (a) $A=3.6\times10^{-7}$ m^2/s and $E_D=12.0$ kJ/mol for hexane data below the melting point and with (b) $A=2.8\times10^{-6}$ m^2/s and $E_D=18.9$ kJ/mol for nitrobenzene data above the melting point.

performed diffusion measurements at $T=265.1$ K *before freezing* (during cooling from $T=340$ K above T_{cr}) and *after melting* (during warming from $T=245$ K after the nitrobenzene-rich phase froze) in the sample with $G24$. Within approximately 5% experimental error, diffusion coefficients are found to be the same (5.1×10^{-10} m^2/s for nitrobenzene and 1.5×10^{-9} m^2/s for hexane). This, in our opinion, further indicates that the structure of the liquid nitrobenzene domains is not altered during freezing.

IV. DISCUSSION

A. Domain-size distributions

The first important conclusion that we can draw from the observation of freezing of the nitrobenzene-rich part in the mixtures imbibed in CPGs of 24−127 nm pore diameters is that the liquid-liquid separation takes place. At the same time we have not measured any observable change of the hexane NMR signal, hence we can conclude that it is true spatial separation of the two liquids that is created before freezing and the observed behavior is not a consequence of nucleation and the ensuing formation of the nitrobenzene crystalline structure from the homogeneous mixture. The occurrence of phase separation in the vicinity of the bulk T_{cr} is also supported by the results of other experimental techniques (dielectric spectroscopy, light scattering) applied to the hexane-nitrobenzene mixture in CPGs of similar pore sizes [2,3]. Consequently, we can regard the experimentally obtained nitrobenzene domain-size distribution functions $P(d)$ in Fig. 3 as reflecting the characteristic size of the phase-separated nitrobenzene-rich domains.

The functions $P(d)$ are found to depend on the pore size of the used porous glasses. Before we start discussing the inter-relation between the structure of CPGs and $P(d)$, we briefly turn to the validity and meaning of the experimentally found distribution functions.

(1) Note that any error introduced in determining the value of K in Eq. (1) [this may come from errors in estimating $\triangle H_f$ and σ or/and from the assumption of the cylindrical morphology for the frozen domains giving a factor of 4 in Eq. (1)] only shifts the distribution functions, but does not change their shape.

(2) Melting of the frozen domains is mostly determined by the minimal characteristic dimension of the crystals. Thus, even if we have an elongated crystal extending over the characteristic pore size, the size obtained by cryoporometry reflects the crystal diameter not length.

(3) It was pointed out that the applicability of the Gibbs-Thompson relation given by Eq. (1) may be questionable for crystals with sizes less than ~10 nm [46,47].

(4) Because of different liquid-wall affinity, the liquid composition might become inhomogeneous over the sample during imbibition. If this would be the case, one could anticipate a bimodal distribution in domain sizes as in Fig. 3(c). However, any such effect is expected to be stronger for the glasses with higher specific surface area or smaller pore size (see Table I), in contrast to our actual observations.

As we have seen in the presentation of results, definitive freezing of the nitrobenzene part in the critical mixture in the porous glass of 7.5-nm pore diameter was not observed. There are two possible explanations of this experimental observation. In Ref. [23], no discernible phase separation for

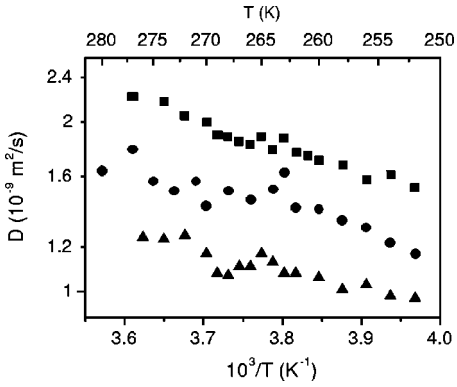

FIG. 6. Average self-diffusion coefficient D_{HX} of hexane in mixtures of different compositions as a function of the temperature at warming in porous glass of 24-nm ($G24$) pore diameter. The nitrobenzene volume fraction ϕ in the mixtures are 0.2 (squares), 0.36 (circles), and 0.6 (triangles).

the aniline-cyclohexane critical mixture in Vycor porous glass of similar pore diameter (7.0 nm) was claimed to be observed. If this is also true for our system, freezing of the nitrobenzene part in the mixture may proceed by nucleation from the homogeneous one-phase mixture with subsequent growth of the nitrobenzene crystals by the diffusion mechanism. However, we did not observe any change of the nitrobenzene-line intensity with time *while keeping the samples at particular temperatures* (recall that measurements were performed in a way to exclude the signal from crystalline phase). This means that the crystal growth supported by diffusion of the nitrobenzene molecules onto crystal surfaces is not observed. On the other hand, even for simple liquids the freezing/melting curve commonly displays a hysteresis loop in pores, with loop width becoming wider with decreasing pore size. This is assumed to be the consequence of liquid-wall interactions. In particular, the freezing/melting behavior of the pure nitrobenzene in CPG (7.5-nm pore diameter) and Vycor (4.0-nm pore diameter) porous glasses has been investigated in Ref. [44] using a DSC method, where it was shown that the hysteresis loop was wider for 4.0-nm pores with continuous freezing until ~ 225 K. In our opinion, this reasonably explains our result for the mixture in $G7$. We claim that the liquid phases separate first below T_{cr} and continuous freezing of the nitrobenzene-rich domains in $G7$ is a consequence of the small pore size. Consequently, we anticipate that the obtained crystal-size distribution function in Fig. 3(a) reflects the actual dimensions of the phase-separated nitrobenzene-rich domains in the liquid state.

We are now ready to discuss the inter-relation between the domain-size distribution functions $P(d)$ and pore sizes. One can see from Fig. 3 that for all samples except $G127$, the dominant distribution mode corresponds to crystal dimensions much less (about half) than the actual pore size. Interestingly, the appearance of the second mode coinciding with the actual pore size is seen clearly in Fig. 3(c) ($G73$). We argue that $G24$ also has this mode: the right wing of $P(d)$ is above the noise level, which is also confirmed by the high-temperature part of the spin-echo intensity curve in Fig. 2(a) that clearly increases with increasing temperature from 263 to 267 K. Although the obtained pore-size distribution function for $G127$ is also asymmetric, it coincides more with the distribution obtained by a one-component liquid.

One of the general features of the distribution functions $P(d)$ obtained in $G7$, $G24$, and $G73$ is the existence of the mode that contains domains much smaller than the dimension of the pores. This finding implies that the (majority of) crystals are rather capsules than plugs in those pores. Note that plugs with merely a few liquidlike monolayers [30,42,48–51] between them and the wall are also inconsistent with the obtained pore-size distribution functions. Hence, phase-separated nitrobenzene domains coexist with the hexane domains on the length scale of and within the pores.

B. Self-diffusion data

The first important conclusion from the self-diffusion data is the confirmation of the absence of macroscopic (on a length scale much above the pore sizes) phase separation in the liquids imbibed in our porous particles. If one assumes a macroscopic phase separation, the volume fraction of the nitrobenzene $\phi_{NB}=0.36$ and the size of the CPG particles ≈ 120 μm (note that only the intra-particle porous volume is saturated) yield an inner phase with size $\geqslant 80$ μm. Using the experimentally measured diffusion coefficients $D_{NB} \approx (0.5\text{–}2)\times 10^{-9}$ m^2/s, one can estimate the molecular displacement for the shortest explored diffusion time $t_d=10$ ms to the order of $\sqrt{6D_{NB}t_d} \leqslant 10$ μm. Hence, we should, in case of macroscopic phase separation, observe nonexponential diffusive decays $S(q,t_d)$ as in bulk mixtures. Instead, single exponential ones were obtained as in Fig. 4 [38,39].

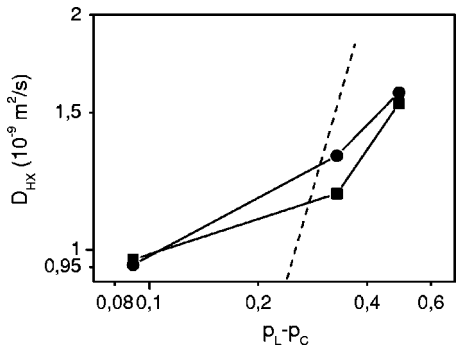

FIG. 7. Self-diffusion coefficient of the hexane molecules D_{HX} vs the volume fraction of hexane p_L-p_C in CPGs of 24-nm ($G24$, squares) and 73-nm ($G73$, circles) pore diameter, using $p_C=0.31$ (see explanations in the text). Equation (7) with $\nu=1.59$ is shown by the dashed line.

On the other hand, at $t_d=160$ ms, displacements of the hexane molecules with the nitrobenzene-rich phase frozen exceed far the pore size. Taking into account the stronger affinity of hexane to the walls [2,44], such long diffusion pathways are accessible for the following morphologies of the nitrobenzene-rich part: (1) capsulelike configurations; (2) tubelike morphologies, that is, capsules extending over many pores; (3) pluglike morphologies with the fraction of the liquid hexane phase above the critical percolation threshold to provide permeation of the liquid molecules throughout CPG particles [52]. The last hypothesis about the plug configuration is not confirmed by the NMR cryoporometry data in Fig. 3 (the mode consistent with plugs became relevant only for large pore sizes). Supporting that the finding is the absence of the appropriate power dependence of D_{HX} on the volume fraction of the liquid phase $p_L \approx 1-\phi_{NB}$ that is typical of diffusion in percolating clusters [52]

$$D \propto (p_L - p_C)^{\nu}, \tag{7}$$

where ν is characteristic of the percolating system and p_C is the threshold value of the percolation network. This can be seen in Fig. 7, where the data taken from Fig. 6 for different values of ϕ_{NB} at $T=250$ K are redrawn using $p_C=0.31$ and compared to the expected (with $\nu=1.59$ [53]) behavior of three-dimensional random site percolation clusters [52].

As we have seen above, during the explored diffusion times t_d the molecules travel over distances that much ex-

ceed the pore size, even with the nitrobenzene-rich phase frozen. Moreover, any dependence $D \propto t_d^k$ with $k<1$, inherent to restricted diffusion, is not observed [31,32]. Thus, we can conclude that the measured values of the diffusion coefficients correspond to their effective long-time values D_∞. The normalized long-time self-diffusion coefficient D_∞/D_0, where D_0 in our case is the diffusion coefficients of pure hexane in CPG, provides a measure of the porous geometry [54]. In our porous glasses where the highly networked porous space for hexane also consists of embedded rigid frozen nitrobenzene crystals, the small change of D_{HX} upon melting of nitrobenzene crystals in Figs. 5 and 6 points to obstruction created by frozen nitrobenzene-rich domains that is comparable to that of liquid nitrobenzene-rich domains as expected on the ground of immiscibility below T_{cr}.

C. Evolution of the liquid-liquid separation

If we assume that all the porous glasses have the same topology, with the sole difference being the size of the structural characteristics such as pore ''bulbs'' and the connecting bottlenecks, the obtained domain-size distribution functions in Fig. 3 suggest the following scenario for the phase transition: First, upon cooling below T_{cr} nitrobenzene droplets are formed in the interior of the pores as a result of random fluctuations. The hexane-rich phase completely wets the surface of the glass. The size of these initial nitrobenzene droplets is small and defined by the nature of the two phase-separating liquids. One can estimate them to be smaller than 5 nm based on the distribution function in Fig. 3(a). For these initial nitrobenzene droplets, the major coarsening mechanism is coalescence through the diffusion of the individual droplets. We suggest that the observed dependence of the size distribution on the pore size is caused by the suppression of such coalescence by the restricting influence of the glass material.

How far droplet coalescence can progress and on which time scale depends on the interplay of several mechanisms. Diffusivity of the individual nitrobenzene droplets D_{dr} decreases inversely in proportion to their size d_{dr} according to the Stokes equation and also depends on the thickness of the wetting layer [9]:

$$D_{dr} \propto \frac{(1-\rho)^2}{\rho^2 d_{dr}}, \tag{8}$$

where $\rho = d_{dr}/d$. As d_{dr} becomes comparable with the pore size d, D_{dr} is substantially suppressed. Additionally, bottlenecks block droplets over a certain size. Further growth can be obtained through Ostwald ripening [55,56] but this mechanism is predicted to be inhibited in pores, particularly in ones prolonged in one dimension such as cylindrical pores [9].

In porous glasses of 7.5- and 24-nm pore diameter with small pores and small bottlenecks, most of the initial droplets within a pore are kept by the bottlenecks for a long enough time to coalesce into a single droplet within the pore [Figs. 3(a) and 3(b)]. On the other hand, the bottlenecks in *G*73 and *G*123 glasses are sufficiently large to let many of the initial droplets pass and thereby some nitrobenzene droplets can grow enough to completely fill some of the pores [Figs. 3(c) and 3(d)].

The validity of these conclusions, derived from the obtained crystal-size distribution functions, depends crucially upon whether or not the structure (morphology and domain-size distribution) of the nitrobenzene-rich domains is preserved during freezing. Our main experimental evidence for this is the behavior on refreezing of the samples. Note that any redistribution of nitrobenzene during freezing is driven by a difference of the nitrobenzene chemical potential μ between frozen and unfrozen nitrobenzene droplets. This, for one solid and one liquid droplet, can be expressed as

$$\triangle H_f \frac{T_m - T}{T_m} + \frac{4\gamma_l}{d_l} - \frac{4\gamma_s}{d_s} = \triangle \mu, \tag{9}$$

where the indices s and l denote the frozen and unfrozen droplets and γ_s and γ_l are the surface energies ($\sigma \equiv \gamma_s - \gamma_l$). With $\triangle \mu > 0$, the liquid droplet may be eliminated by molecular diffusion from liquid to the solid droplet. Since $T \approx T_m$, the dominant driving force for this is the size difference between the droplets. Hence, as long as a size distribution of domains exists repeated freezing/melting should lead to a diminishing fraction of small domains. Our experimental evidence (unchanged size distribution obtained by repeated freezing/melting) does not support such a scenario, from which we conclude that freezing keeps the spatial distribution of the nitrobenzene domains intact. This conclusion is further supported by computer simulation studies that yield a very slow growth by molecular diffusion of the minority domains in the pores at temperatures below T_{cr} [9–12,18].

V. CONCLUSIONS

In this work low-temperature phase separation of the binary nitrobenzene-hexane liquid in porous glasses with controlled pore sizes from 7.5 to 127 nm is studied. It is shown that the applied cryoporometry and diffusion NMR methods give new insight to details of the liquid-liquid coexistence in pores and essentially complement the data obtained by other experimental techniques such as light [1,4–7,22] and neutron [19,20] scattering, NMR spectroscopy [23,24], and nonlinear dielectric response [2,3]. Being free of the background scattering problem from the solid host, inherent to scattering methods, NMR-based methods allow obtaining direct information on mixture properties itself.

The NMR cryoporometry method utilizes the shift in the melting temperature of frozen crystals due to their finite size. Its application to investigation of the structure of phase-separated liquids, which recently has been proposed in Ref. [26], crucially depends on two suppositions: (1) frozen crystals in pores are formed by freezing of one of the liquid-liquid separated component, not by nucleation and crystal growth from the homogeneous one-phase liquid; (2) during freezing of the phase-separated liquid domains, their morphological properties remain unchanged. We show from our experimental data, substantially complemented with information on molecular diffusion, that these suppositions hold

at least for mixtures in 24 nm and larger size porous glasses. It is also anticipated that they are satisfied in 7.5-nm pores, but additional experiments are required to provide the final answer. This could be done, for example, by performing transverse NMR relaxation measurements during freezing/melting of the frozen domains.

With these two conditions satisfied, some general conclusions that are consistent with the previous experimental studies can be drawn. First, the diffusion data reveal that *macrophase* separation is not reached on the explored time scale (many hours). At the same time, freezing of one of the mixture components, reflected by disappearance of its line in the NMR spectra, points out that liquid-liquid *microphase* separation has taken place on the pore length scale. Specifically, the nitrobenzene-rich domains occupy the interior of the pores, while hexane-rich phase wets the glass surface.

Additionally, some other features have been found. The strong relationship between the melting temperature and the crystal size according to Eq. (1) allowed us to derive the domain-size distribution function of the minority phase. Similar characteristics for phase-separating liquids has been found before using confocal microscopy, but only for bulk mixtures containing one polymer component [57,58]. The dependence of the found distribution functions on the pore size reveals that late-stage formation of the separated phases is crucially controlled by the morphology of the porous space. We suggest that it is caused by the inter-relation between two physical properties of the system: (1) Diffusion of the small droplets of the minority phase, formed at cooling below T_{cr}, and being the major coarsening mechanism at the late stages of spinodal decomposition; and (2) specific properties of the porous morphology as pore bottlenecks and pore junctions, controlling the droplets coalescence. Our experimental finding that the domain-size distribution functions *do not depend* on exposure time from minutes to a few hours at temperatures below T_{cr} before freezing indicates fast local equilibration on the pore length scale. Note that redistribution of the droplets through their diffusion is not directly accounted for neither in RFIM [15,16], nor in SPM [17]. Thus, in the treatment of experimental results one should keep in mind that the real picture of the phase separation in random pores may be substantially shifted from the predictions of these theoretical models. One should also note that within our droplet coalescence model the minority domains are rather short capsules than tubes that extend over several characteristic pore lengths; these two scenarios are otherwise indistinguishable on the basis of our experimental data.

The interplay between the dynamical properties of the phase-separating liquids and structural parameters of the porous materials may lead to the bimodal domain-size distribution observed in this study. Despite many computer simulations having been done concerning binary liquids under confinement, bimodal distributions have never been observed. In our opinion, this is probably a consequence of using idealized models of the porous space, such as tube, parallelepiped, or parallel sheets (see, for example, Refs. [9,10,14,18] and references therein). A few computer studies dealing with more realistic pore models resembling Vycor-like porous glasses introduced new observations with respect to the idealized models [11–13]. At the same time the results obtained using a Cahn-Hilliard description [11,12] and a lattice Boltzmann method [13] were in contradiction. In the former it was established that interconnected and tortuous porous structure causes a presence of many length scales in the system and breaking down of the dynamical scaling. In the latter, authors concluded that late-stage decomposition is irrelevant to the form of the confining geometry. All of these certainly show that the details of porous morphology affect the properties of phase separation.

ACKNOWLEDGMENTS

This project has been supported by the Swedish Foundation for Strategic Research SSF (''Paper surfaces for digital printing''), the Swedish Research Council VR, and CRDF through Grant No. REC-007. We also thank John Daicic for useful discussions and suggestions.

[1] M.C. Goh, W.I. Goldburg, and C.M. Knobler, Phys. Rev. Lett. **58**, 1008 (1987).
[2] M. Sliwinska-Bartkowiak, S.L. Sowers, and K.E. Gubbins, Langmuir **13**, 1182 (1997).
[3] M. Sliwinska-Bartkowiak, R. Sikorski, S.L. Sowers, L.D. Gelb, and K.E. Gubbins, Fluid Phase Equilibria **136**, 93 (1997).
[4] S.B. Dierker and P. Wiltzius, Phys. Rev. Lett. **58**, 1865 (1987).
[5] P. Wiltzius, S.B. Dierker, and B.S. Dennis, Phys. Rev. Lett. **62**, 804 (1989).
[6] S.B. Dierker and P. Wiltzius, Phys. Rev. Lett. **66**, 1185 (1991).
[7] S.B. Dierker, B.S. Dennis, and P. Wiltzius, J. Chem. Phys. **92**, 1320 (1990).
[8] L.D. Gelb, K.E. Gubbins, R. Radhakrishnan, and M. Sliwinska-Bartkowiak, Rep. Prog. Phys. **62**, 1573 (1999).
[9] L. Monette, A.J. Liu, and G.S. Grest, Phys. Rev. A **46**, 7664 (1992).
[10] L.D. Gelb and K.E. Gubbins, Phys. Rev. E **56**, 3185 (1997).
[11] A. Chakrabarti, Phys. Rev. Lett. **69**, 1548 (1992).
[12] Z. Zhang and A. Chakrabarti, Phys. Rev. E **52**, 2736 (1995).
[13] D.W. Grunau, T. Lookman, S.Y. Chen, and A.S. Lapedes, Phys. Rev. Lett. **71**, 4198 (1993).
[14] K. Binder, J. Non-Equilib. Thermodyn. **23**, 1 (1998).
[15] F. Brochard and P.G. de Gennes, J. Phys. (France) Lett. **44**, 785 (1983).
[16] P.G. de Gennes, J. Phys. Chem. **88**, 6469 (1984).
[17] A.J. Liu, D.J. Durian, E. Herbolzheimer, and S.A. Safran, Phys. Rev. Lett. **65**, 1897 (1990).
[18] A.J. Liu and G.S. Grest, Phys. Rev. A **44**, 7894 (1991).
[19] F. Formisano and J. Teixeira, Eur. Phys. J. E **1**, 1 (2000).
[20] F. Formisano and J. Teixeira, J. Phys.: Condens. Matter **12**, A351 (2000).
[21] A. Maritan, M.R. Swift, M. Cieplak, M.H.W. Chan, M.W. Cole, and J.R. Banavar, Phys. Rev. Lett. **67**, 1821 (1991).

[22] M.Y. Lin, S.K. Sinha, J.M. Drake, X.-L. Wu, P. Thiyagarajan, and H.B. Stanley, Phys. Rev. Lett. **72**, 2207 (1994).
[23] S. Lacelle, L. Tremblay, Y. Bussiere, F. Cau, and C.G. Fry, Phys. Rev. Lett. **74**, 5228 (1995).
[24] L. Tremblay, S.M. Socol, and S. Lacelle, Phys. Rev. E **61**, 656 (2000).
[25] H. Tanaka, J. Phys.: Condens. Matter **13**, 4637 (2001).
[26] R. Valiullin and I. Furó, J. Chem. Phys. **116**, 1072 (2002).
[27] C.L. Jackson and G.B. McKenna, J. Chem. Phys. **93**, 9002 (1990).
[28] M. Brun, A. Lallemand, J.-F. Quinson, and C. Eyraud, Thermochim. Acta **21**, 59 (1977).
[29] J.H. Strange, M. Rahman, and E.G. Smith, Phys. Rev. Lett. **71**, 3589 (1993).
[30] K. Overloop and L. Van Gerven, J. Magn. Reson. A **101**, 179 (1993).
[31] P.T. Callaghan, *Principles of Nuclear Magnetic Resonance Microscopy* (Clarendon Press, Oxford, 1991).
[32] J. Kärger and M. Ruthven, *Diffusion in Zeolites* (Wiley, New York, 1992).
[33] A.V. Filippov and V.D. Skirda, Colloid J. USSR **62**, 837 (2000).
[34] K. Tang, C. Zhou, X. An, and W. Shen, J. Chem. Thermodyn. **31**, 943 (1999).
[35] C. Faivre, B. Dellet, and G. Dolino, Eur. Phys. J. B **7**, 19 (1999).
[36] P. Stilbs, Prog. Nucl. Magn. Reson. Spectrosc. **19**, 1 (1987).
[37] D. Wu, A. Chen, and C.S. Johnson, Jr., J. Magn. Reson. A **115**, 260 (1995).
[38] A.I. Maklakov, V.D. Skirda, and N.F. Fatkullin, in *Encyclopedia of Fluid Mechanics*, edited by N.P. Cheremisinoff (Gulf-Publishing Co., Houston, 1990), Chap. 22, pp. 705–745.
[39] A.R. Waldeck, P.W. Kuchel, A.J. Lennon, and B.E. Chapman, Prog. Nucl. Magn. Reson. Spectrosc. **30**, 39 (1997).
[40] D.R. Douslin and H.M. Huffman, J. Am. Chem. Soc. **68**, 1704 (1946).
[41] G.S. Parks, S.S. Todd, and W.A. Moore, J. Am. Chem. Soc. **58**, 398 (1936).
[42] M. Sliwinska-Bartkowiak, G. Dudziak, R. Sikorski, J. Gras, R. Radhakrishnan, and K.E. Gubbins, J. Chem. Phys. **114**, 950 (2001).
[43] D. Costa, P. Ballone, and C. Caccamo, J. Chem. Phys. **116**, 3327 (2002).
[44] M. Sliwinska-Bartkowiak, J. Gras, R. Sikorski, R. Radhakrishnan, L. Gelb, and K.E. Gubbins, Langmuir **15**, 6060 (1999).
[45] E. Hawlicka and W. Reimschüssel, Ber. Bunsenges. Phys. Chem. **85**, 210 (1981).
[46] H. Sakai, Surf. Sci. **351**, 285 (1996).
[47] Q. Jiang, H.X. Shi, and M. Zhao, J. Chem. Phys. **111**, 2176 (1999); Q. Jiang, L.H. Liang, and M. Zhao, J. Phys.: Condens. Matter **13**, L397 (2001).
[48] R. Kimmich, S. Stapf, A.I. Maklakov, V.D. Skirda, and E.V. Khozina, Magn. Reson. Imaging **14**, 793 (1996).
[49] S. Stapf and R. Kimmich, Chem. Phys. Lett. **275**, 261 (1997).
[50] D.W. Aksnes, L. Gjerdåker, S.G. Allen, H.F. Booth, and J.H. Strange, Magn. Reson. Imaging **16**, 579 (1998).
[51] K. Morishige and K. Kawano, J. Chem. Phys. **110**, 4867 (1999).
[52] D. ben-Avraham and S. Havlin, *Diffusion and Reactions in Fractals and Disordered Systems* (Cambridge University Press, Cambridge, 2000).
[53] H.P. Müller, R. Kimmich, and J. Weis, Phys. Rev. E **54**, 5278 (1996).
[54] R. Valiullin and V. Skirda, J. Chem. Phys. **114**, 452 (2001).
[55] J. Schmelzer, J. Möller, and V.V. Slezov, J. Phys. Chem. Solids **56**, 1013 (1995).
[56] J. Bibette, F. Leal-Calderon, and P. Poulin, Rep. Prog. Phys. **62**, 969 (1999).
[57] W.R. White and P. Wiltzius, Phys. Rev. Lett. **75**, 3012 (1995).
[58] B.V.R. Tata and B. Raj, Bull. Mater. Sci. **21**, 263 (1998).